TÜBİTAK

Turkish Journal of Physics

http://journals.tubitak.gov.tr/physics/

Research Article

Turk J Phys
(2023) 47: 12 – 27

doi:10.55730/1300-0101.2735

Speeding the generation of giant entangled states using low-frequency modulations

Abdelaziz BENSEGHIR[1], Azeddine MESSIKH[2,*], Ahmed BOUKETIR[3]
[1]Department of Physics, Laboratory of Applied Sciences and Didactic,
Ecole Normale Superieure Laghouat (ENSL), Algeria
[2]Semiconductors Technology Research Center for Energetics, Algiers, Algeria
[3]Department of Mathematical Sciences, Dammam Community College,
King Fahd University of Petroleum and Minerals, Dhahran, Saudi Arabia

Received: 09.09.2022 • **Accepted/Published Online:** 24.01.2023 • **Final Version:** 23.02.2023

Abstract: In this paper, we generalize the shortcuts to adiabacity for the quantum Rabi model by simultaneously modulating its two components, namely, the two-level system and the cavity mode. This will eliminate the counterrotating terms which in turn helps to simulate the Rabi model by the Jaynes-Cummings model without requiring a largely detuned light-matter coupling. We focus on the low-frequency modulations since it is easy to realize them experimentally. The results show that these modulations can significantly shorten the evaluation time, generate much larger entanglement cat states, and robust against imperfection of time evaluation and dissipation.

Keywords: Shortcuts to adiabacity, Rabi model, cat states, ultrastrong coupling

1. Introduction

The quantum Rabi model [1, 2] is the simplest light-matter interaction in quantum physics and has many applications in quantum optics [3], condensed matter physics [4, 5], and quantum information [6]. In 2011 Braak [7] found that it is exactly solvable. The Rabi model can be divided into different regimes depending on the normalized coupling strength η, the ratio between the coupling strength and the system frequencies [8], and the dissipation rates. Two of these regimes are of great importance: ultrastrong coupling and deep-strong coupling. The ultrastrong coupling (USC) regime occurs when the coupling strength between light and matter is comparable to the atomic or cavity frequencies, $\eta \approx 0.1 \sim 1$. This regime has attracted increasing attention since its first observation in the microcavity-embedded doped GaAs quantum well [9]. Later, a broad range of physical systems have been used to demonstrate it, including light-molecule [10], cavity quantum electrodynamics (QED) systems [9, 11], and circuit-QED systems [12]. The deep-strong regime occurs when the coupling strength becomes larger than 1, $\eta \gtrsim 1$. A value of $\eta = 1.34$ was obtained experimentally in 2017 [13, 14]. Such a regime would be of great significance for generating maximally entangled cat states.

It is well known that for small values of η the rotating wave approximation is valid, and the Rabi

*Correspondence: amessikh@yahoo.com

model can be simplified to the Jaynes-Cummings (JC) model [15], where the counter-rotating terms are ignored. Recently, an interesting idea has been proposed to realize the JC model in the ultrastrong regime [16]. It is an important way to demonstrate that the JC model and the ultrastrong coupling regime can coexist simultaneously. This proposed model does not rely directly on the rotating wave approximation but rather on modulating the frequencies of the two-level system and the bosonic mode. The frequency modulation of the two-level system can be realized experimentally using a longitudinal driving field [17–19], while the modulation of the cavity can be implemented by using a superconducting quantum interference device (SQUID) [20–22]. It was shown that for appropriate modulations, the counterrotating terms can be completely suppressed in high and low frequency modulations without the need to reduce the coupling strength of the Rabi model. This new idea opens a new way to implement ultrafast quantum state transfer, ultrafast quantum logic gates [23], and to demonstrate the quantum phase transition [16].

Shortcuts to adiabaticity is a general approach to accelerate slow adiabatic processes and leads to fast nonadiabatic evolution. It is based on adding a suitable counterdiabatic Hamiltonian to the original time-dependent Hamiltonian to suppress transitions between the instantaneous eigenbasis. It has been applied in many fields, especially in fast quantum information processing [24–26]. An interesting model based on shortcuts to adiabaticity has been recently proposed to generate giant entangled cat states [27]. The entangled cat states with large size are very important in quantum information, especially in quantum metrology [28], quantum processing [29], and fault-tolerant quantum computation [30, 31]. The proposed model is based on a parametric amplification process utilizing a χ^2-nonlinear medium which is driven by two-photon time-dependent coherent fields. One of these fields is used to produce a time-dependent squeezed-cavity mode and the other, which is $\pi/2$-phased from the first one, is used to suppress transitions between different time-dependent eigenstates and thus prevents nonadiabatic transitions. This is one of the well known shortcuts to adiabatic methods. Such methods are used to mimic adiabatic evolution beyond the adiabatic limit [32–34], which in turn speed up the quantum adiabatic process. In order to reduce the influence of the cavity loss in this model, a broadband squeezed vacuum generated from an optical parametric amplifier is used. It was shown that this interesting model is much faster than its adiabatic counterpart which requires a long-time evolution. In addition, it is robust against dissipation and imperfection of the evolution time when the detuning is very large.

Speeding up the generation of entangled state is very crucial in quantum information. Recently, Yan et.al. [35] have proposed an effective scheme for speeding up the generation of an entangled state between superconducting qubit and cavity photons via counterdiabatic driving, which is one of the STA methods. They have used a three-level system in Λ-configuration. Driving it by external time-dependent fields and a quantized cavity mode using adiabatic population transfer leads to an entangled state; then an extra field, counterdiabatic driving, is used to speed up this generated entangled state. Motivated by the possibility of speeding up an entangled state with a large mean photon number, we extend the work of Ref. [27] by simultaneously modulating the two-level system and the cavity mode in the low-frequency modulations. These modulations which eliminate the counterrotating terms overcome the condition proposed in Ref. [27] and therefore can greatly shorten the evolution time of the shortcuts to adiabatic protocol and increase the size of the generated entangled cat states. We also study the time required to obtain these giant entangled cat states and their robustness against time evolution imperfection and dissipation. The rest of the paper is organized as follows: In Section 2, we review the ultrastrong JC model [16] with the generalized Rabi model where the quadratic term is

taken into account. In Section 3, we generalize the shortcuts to adiabaticity [27] by using low-frequency modulations and show that these modulations improve the generation of nonclassical ground state in terms of speed and size. We also discuss its robustness to the imperfection of time evolution. A conclusion is given in Section. 5.

2. Simulation of the generalized Rabi model

The standard Hamiltonian of the quantum Rabi model is given by

$$H_R = \frac{\omega_a}{2}\sigma_z + \omega_c a^\dagger a + g\sigma_x\left(a^\dagger + a\right), \tag{2.1}$$

where ω_a is the frequency of the two-level system, ω_c is the frequency of the cavity mode, $\sigma_{x(z)}$ is the well known Pauli operator, $a(a^\dagger)$ is the annihilation (creation) operator of the cavity mode, and g is the coupling strength. It is worth mentioning that the derivation of this Hamiltonian is based on the electron-electromagnetic field interaction without the quadrature term. It was shown that this quadratic term can have significant effects on quantum state transfer and nonclassical quantum state preparation in the strong and ultrastrong coupling regimes. The Rabi model with this quadrature term is called the generalized Rabi model and its Hamiltonian is then written as [36]

$$H = \frac{\omega_a}{2}\sigma_z + \omega_c a^\dagger a + g\sigma_x\left(a^\dagger + a\right) + \frac{1}{2}g\zeta\left(a^\dagger + a\right)^2. \tag{2.2}$$

Here, ζ is a dimensionless parameter that characterizes the strength of the quadrature term and its value depends on the system in consideration. For example, its maximum value is close to 3 for the cooper pair-transmission-line-resonator (TLR) system [37]. Due to the counterrotating terms, the Hamiltonian H does not conserve the excitation number operator $N_e = a^\dagger a + \sigma_+\sigma_-$, where $\sigma_{+(-)}$ is the raising (lowering) operator. However, under the rotating wave approximation, where the coupling strength is $g \ll \{\omega_a, \omega_c\}$, these counterrotating terms do not contribute to the evolution of the system and the Hamiltonian H reduces to

$$H_{\text{RWA}} = \frac{\omega_a}{2}\sigma_z + (\omega_c + g\zeta)\, a^\dagger a + g\left(\sigma_- a^\dagger + \sigma_+ a\right). \tag{2.3}$$

It is clear from the previous equation that the quadratic term has the effect of shifting the frequency of the cavity mode by an amount of $g\zeta$. This shifting should be taken into consideration in case the quadrature term is significant.

In the case that the rotating wave approximation is not valid, the counterrotating terms play an essential part in the evolution. To deal with these terms, we follow Ref. [16] and write the Hamiltonian (2.2) as the sum of two Hamiltonians

$$H = H_{\text{RWA}} + H_{CR}, \tag{2.4}$$

where H_{CR} includes all the counterrotating terms as well as the quadrature term

$$H_{CR} = g\left(\sigma_+ a^\dagger + \sigma_- a\right) + \frac{1}{2}g\zeta\left(a^{\dagger 2} + a^2\right). \tag{2.5}$$

By applying a pair of sinusoidal frequency modulations to the two-level system and the cavity mode, the frequencies ω_a and ω_c in Equation (2.3) are chosen to be time-dependent according to the following equations

$$\omega_a(t) = \omega_a + \xi\nu\cos(\nu t), \tag{2.6}$$
$$\omega_c(t) = (\omega_c + g\zeta) + \xi\nu\cos(\nu t). \tag{2.7}$$

Here, ξ and ν are positive real numbers correspond to the amplitude and frequency modulations. It is convenient to work in the rotating frame defined by the unitary transformation

$$\begin{aligned} U(t) &= \exp\Big\{ i\left[(\omega_c + g\zeta)\, t + \xi\sin(\nu t)\right] a^\dagger a + \\ &\quad i\left[\omega_a t + \xi\sin(\nu t)\right]\sigma_z/2\Big\}. \end{aligned} \tag{2.8}$$

In this frame the Hamiltonian takes the form

$$\begin{aligned} H^I &= UHU^\dagger + i\dot{U}U^\dagger, \\ &= g\left(\sigma_- a^\dagger \mathrm{e}^{-i\delta t} + \sigma_+ a \mathrm{e}^{i\delta t}\right) \\ &\quad + g\left(\sigma_+ a^\dagger\ \mathrm{e}^{i(\omega_a+\omega_c+g\zeta)t}\ \mathrm{e}^{2i\xi\sin(\nu t)} + \mathrm{h.c.}\right) \\ &\quad + \frac{1}{2} g\zeta\left(a^{\dagger 2}\ \mathrm{e}^{2i(\omega_c+g\zeta)t}\ \mathrm{e}^{i2\xi\sin(\nu t)} + \mathrm{h.c.}\right), \end{aligned} \tag{2.9}$$

where $\delta = \omega_a - \omega_c - g\zeta$. The extra term $g\zeta$ reflects the role of the quadrature term in both rotating and counterrotating terms.

There are two interesting regions where we can get rid of the counterrotating terms as was mentioned in [16].

(i) The high-frequency modulation regime: Using the well know Jacobi-Anger identity

$$\mathrm{e}^{2i\xi\sin(\nu t)} = \sum_{n=-\infty}^{\infty} J_n(2\xi)\mathrm{e}^{in\nu t}, \tag{2.10}$$

where J_n is the Bessel function of the first kind, one can put

$$H^I = H^I_{JC} + \epsilon(t), \tag{2.11}$$

with

$$H^I_{JC} = g\left(\sigma_- a^\dagger \mathrm{e}^{-i\delta t} + \sigma_+ a \mathrm{e}^{i\delta t}\right), \tag{2.12}$$

$$\begin{aligned} \epsilon(t) &= g\Bigg[\sigma_+ a^\dagger \sum_{n=-\infty}^{\infty} J_n(2\xi)\mathrm{e}^{i\Delta_{1n}t} + \\ &\quad \frac{\zeta}{2}\, a^{\dagger 2} \sum_{n=-\infty}^{\infty} J_n(2\xi)\mathrm{e}^{i\Delta_{2n}t} + \mathrm{h.c.}\Bigg], \end{aligned} \tag{2.13}$$

where $\Delta_{1n} = \omega_a + \omega_c + g\zeta + n\nu$ and $\Delta_{2n} = 2(\omega_c + g\zeta) + n\nu$. By choosing large values of $|\Delta_{1,2n}| \gg 1$, the fast oscillating terms can be dropped, and to eliminate the term corresponding to $n = 0$, we take $\xi = 2.76$ which leads to zero Bessel function J_0. In this case, the total Hamiltonian H is reduced to the Jaynes-Cummings Hamiltonian (2.12), $H^I \approx H^I_{JC}$.

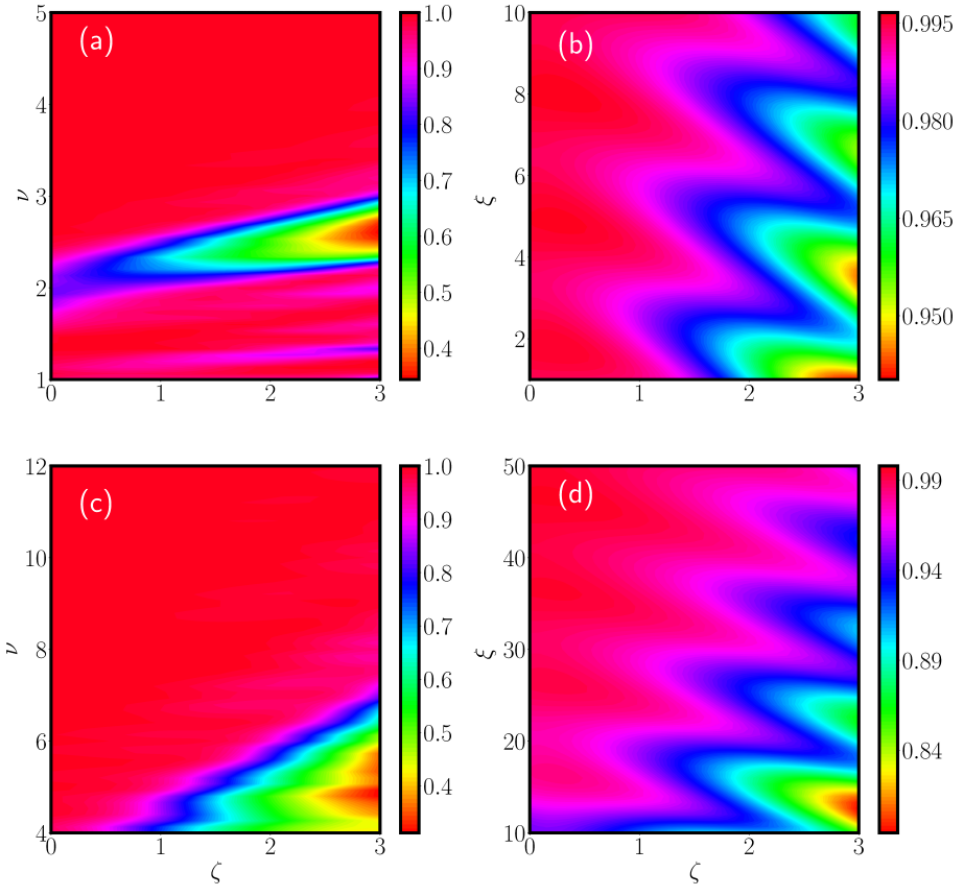

Figure 1. The Fidelity at $t = \pi/(2g)$ for two different values of g. The panels (a) and (c) are for high-frequency modulations ($\nu > 1$) with $g = 0.1$ and $g = 0.5$, respectively. The panels (b) and (d) are for low-frequency modulations ($\nu = 0.1$) with $g = 0.1$ and $g = 0.5$, respectively. The other parameters are: $\omega_a = \omega_c = 1$ and the initial state is $(|g\rangle + |e\rangle)\,|\alpha\rangle/\sqrt{2}$ with $\alpha = 0.1$. The red region is the region where the fidelity is close to 1, i.e. the counterrotating terms has no influence on the system evolution. In high-frequency modulations, the parameter is chosen $\xi = 2.76$ to eliminate the Bessel function, i.e. $J_0(2\xi) = 0$.

(ii) The low-frequency modulation regime: In case $\nu \ll \omega_a$ and for short time evolution, the approximation $\sin(\nu t) \approx \nu t$ is used. If we choose ξ such that the frequencies are much larger than the coupling strength, the total Hamiltonian can be also reduced to the Jaynes-Cummings Hamiltonian.

To evaluate the validity of these approximations in high(low)-frequency modulations we compute the fidelity

$$F(t) = |\langle\phi(t)|\psi(t)\rangle|^2, \tag{2.14}$$

where $|\phi(t)\rangle$ is the solution of the Schrödinger equation for the total Hamiltonian (2.2) and $|\psi(t)\rangle$ for the JC Hamiltonian (2.3), taking into account that the frequencies are now time-dependent according to Equation (2.6). In Figure 1, we plot the fidelity at $t = \pi/(2g)$ and for two different coupling strengths $g = 0.1$ and $g = 0.5$. The initial state is chosen to be $(|g\rangle + |e\rangle)|\alpha\rangle/\sqrt{2}$, where $|g(e)\rangle$ is the ground (excited) state of the two-level system and $|\alpha\rangle$ is the coherent state with $\alpha = 0.1$. For simplicity, we consider only the resonance case $\omega_a = \omega_c = 1$. Figures 1a and 1c are for high-frequency modulations ($\nu > 1$) with $\xi = 2.76$ which eliminate the Bessel function, $J_0(2\xi) = 0$. Figures 1b and 1d are for low-frequency modulations with $\nu = 0.1$. It is clear from these figures that for high(low)-frequency modulations the fidelity is close to 1 (red color regions) for large values of $\nu(\xi)$. For low-frequency modulation the strength of the quadrature term ζ should be small enough to have a fidelity close to 1. Figures 1a and 1c also show that in order to have a fidelity close to 1 for large Rabi frequency g the parameter ν should be large enough. That is, the higher the value of the Rabi frequency, the more we need to increase the frequency modulation ν. Similarly for low-frequency modulations, increasing the Rabi frequency needs to use larger values of ξ.

By choosing the values of the tuner parameters (the red region in Figure 1), it is possible to completely suppress the effect of H_{CR} and the generalized Rabi model behaves like the JC model with a shift in the cavity frequency by an amount of $g\zeta$. It is worth mentioning here that for small coupling strength the generalized Rabi model can be approximated by the JC model using the rotating wave approximation. With these modulations, we can go beyond this approximation and thus, our approach is valid for arbitrary values of the coupling strength.

3. Shortcuts to adiabaticity with low-frequency modulations

In this section, we generalize the shortcuts to adiabatic method [27] by focusing on the low-frequency modulations technique. To realize that, we choose the parameters in the region where $H \approx H_{\text{RWA}}$ (see the red regions in Figure 1). So, the Hamiltonian Equation (2.3) can be written in the rotating frame as

$$H \approx \Delta a^\dagger a + g\left(\sigma_- a^\dagger + \sigma_+ a\right), \tag{3.1}$$

with $\Delta = \omega_c - \omega_a + g\zeta$. To generate an entangled state a χ^2-nonlinear medium is inserted into the cavity and two nonlinear time-dependent drive this medium. One of them $\Omega_r(t)$ induces a squeezed-cavity mode and the other $\Omega_i(t)$ is used to counteract the nonadiabatic transition. Therefore, the Hamiltonian becomes

$$H_0(t) = \Delta a^\dagger a - \left[\frac{\Omega_r(t) + i\Omega_i(t)}{2} a^2 - g a^\dagger \sigma_- + \text{h.c.}\right], \tag{3.2}$$

where we have assumed that both fields have the same time-dependent phase $\omega_p(t) = 2\left(\omega_a t + \xi \sin(vt)\right)$. In low-frequency modulations, $\nu t \ll 1$, the common frequency has a simple formula $\omega_p = 2\left(\omega_a + \xi v\right)$. In what follows we will focus only on the low-frequency modulation and we will not consider the high-frequency modulation. This is due to the fact that low-frequency modulation is more accessible experimentally than the high-frequency modulation [16].

At this point, it is convenient to work in the squeezing frame rather than in the lab frame. Therefore, the effective Hamiltonian can be written in the form [27]

$$\begin{aligned} H_S &= S^\dagger(t)HS(t) - iS^\dagger(t)\dot{S}(t), \\ &= \Delta \text{sech}[2r(t)]a^\dagger a + \frac{g}{2}\exp[r(t)](a^\dagger + a)\sigma_x - \\ &\quad i\frac{g}{2}\exp[-r(t)]\sigma_y(a^\dagger - a), \end{aligned} \tag{3.3}$$

where the unitary transformation is given by the squeezed operator $S(t) = \exp\left[r(t)(a^{\dagger 2} - a^2)/2\right]$, and $r(t)$ is a real squeezing parameter with time-dependent given by

$$r(t) = \frac{r_{\max}}{1 + \exp\{f(t)\}}, \tag{3.4}$$

where $r_{\max}$ is the maximum value of the squeezing parameter, $f(t) = f_0 \cos(2\pi t/T)$ with $f_0 \gg 1$, and T is the duration of the evolution. For a feasible gain of 20 dB, the value of $r_{\max}$ is approximately equal to 2.3 [38, 39]. This is the value that we use in our numerical calculations. Note that the time-dependent of $r(t)$ is chosen so that $r(T) \approx 0$. Thus, at the end of the evolution the state in the squeezing frame is the same as in the lab frame. We should emphasis here that in Ref. [27] the last term in (3.3), $H_{err} = -i\frac{g}{2}\exp[-r(t)]\sigma_y(a^\dagger - a)$, is considered as an error term since the detuning takes

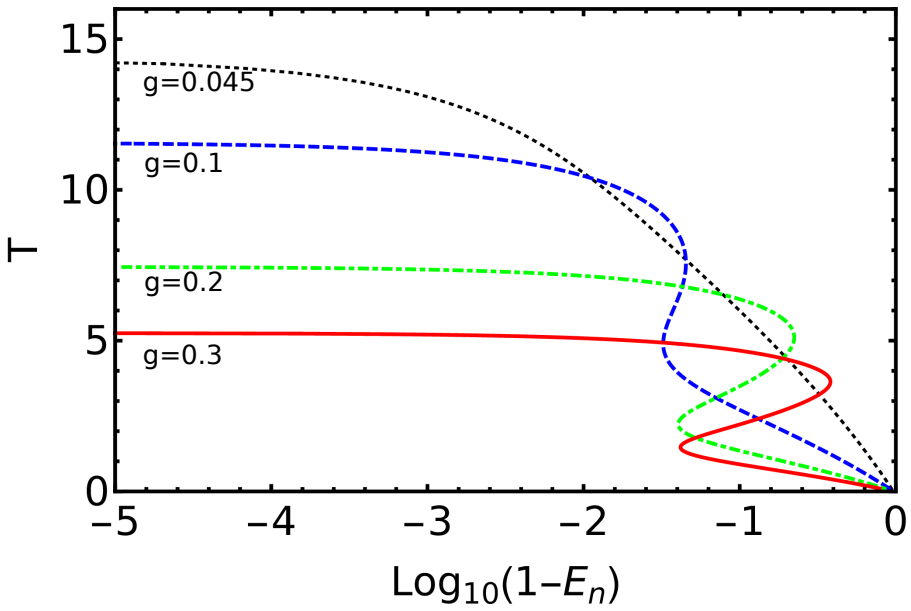

Figure 2. The shortest time evolution T as a function of the logarithmic negativity at low-frequency modulations in the presence of the error term H_{err} and for different values of the coupling strength g. The parameters are: $\Delta = 1$, $r_{\max} = 2.3$, and $f_0 = 10$. The initial state is given by Eq. (3.5) with $\eta(0) = (1+i)/100$. To achieve $E_n \gtrsim 99.99\%$ for $g \in (0.045, 0.1, 0.2, 0.3)$, one needs the evolution time $T \sim (14.2, 11.6, 7.5, 5.3)$.

a much larger value than the coupling strength, $|g/\Delta| \ll 1$. However, with frequency modulations it is possible to go beyond this condition and the ratio $|g/\Delta|$ can take any value. Thus, the term H_{err} is no longer negligible in our case and can affect the generation of the entangled cat states.

Figure 2 displays the dependence of the logarithmic negativity $E_n = \log_2 \left\|\rho^{\Gamma_q}\right\|_1$, which is an entanglement measure, on the evolution time T for different values of Rabi frequency g and initial state

$$|\psi(0)\rangle = \frac{1}{\sqrt{2}}\left(|+\rangle_x|-\eta(0)\rangle + |-\rangle_x|\eta(0)\rangle\right), \tag{3.5}$$

where, $|\pm\rangle_x$ are the eigenstates of the Pauli operator σ_x and $\eta(0) = (1+i)/100$ is a complex number. The symbol Γ_q means the partial transpose operation with respect to the two-level system space, and $\|.\|_1$ denotes the trace norm. This figure shows the effect of overcoming the detuning condition $\Delta/g \gg 1$ posed in [27]. It is clear that increasing the coupling strength speeds the generation of the entangled cat states. Therefore, to achieve $E_n \gtrsim 99.99\%$ for $g \in (0.045, 0.1, 0.2, 0.3)$, one needs the evolution time $T \sim (14.2, 11.6, 7.5, 5.3)$.

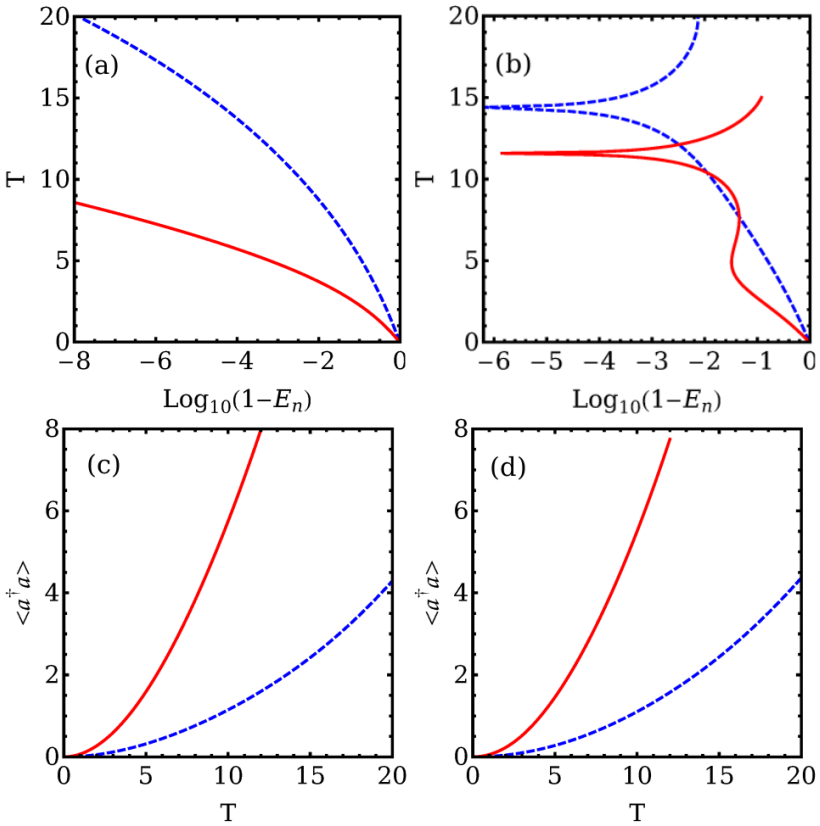

Figure 3. The logarithmic negativity and the mean photon number without ((a) and (c)) and with ((b) and (d)) the error term H_{err}. The parameters are: $\Delta = 1$, $r_{\max} = 2.3$, and $f_0 = 10$. The initial state is given by Eq. (3.5) with $\eta(0) = (1+i)/100$. Solid line with low frequency modulations for $g = 0.1$ and dashed line for $g = 0.045$. The frequency modulations shorten the required time to obtain entangled cat state.

Figure 3 focuses on g = 0.1 and g = 0.045 in order to keep the effect of H_{err} small but not negligible and to compare with Ref. [27]. It shows that applying frequency modulations increases the mean photon number, as well as reducing the evolution time. Also, one can notice that the term H_{err} does not affect the behavior of the mean photon number which grows exponentially with the evolution time, but it affects the negativity. In the case that this term is taken into account, the logarithmic negativity is no longer a monotonic function of time evolution; instead there are collapses and revivals of entanglement starting from the shortest time. Since we are interested in the smallest time, the calculations with H_{err} lead to a longer time evolution (T = 11.57) than without it (T = 8.60) for $g = 0.045$ and the mean photon number in our case is 7.23 which is larger than 4.3 found in Ref. [27].

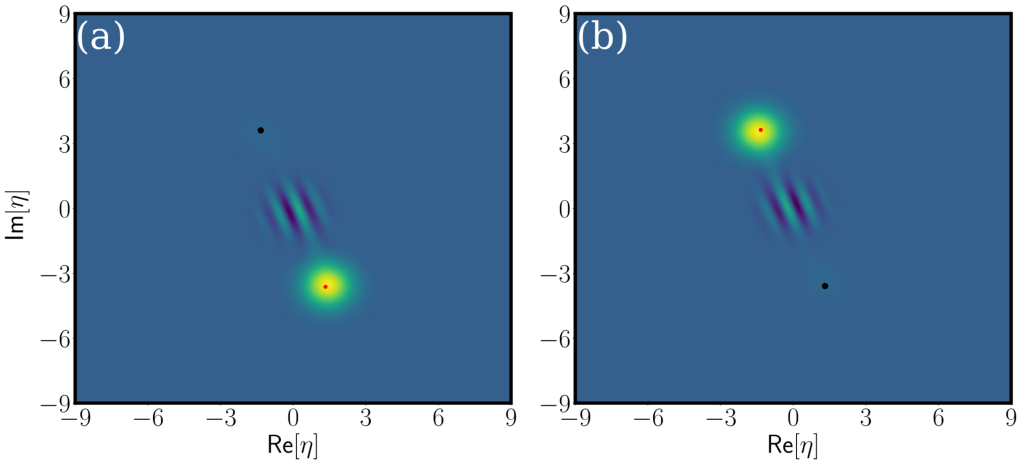

Figure 4. Wigner function of the projection on the eigenstates of the Pauli operator σ_x. (a) for the projection on $|-\rangle_x$ and (b) on $|+\rangle_x$. The red (black) dot corresponds to the solution of the differential equations (3.7). The spots in (a) and (b) are symmetric with respect to the origin.

To visualize the state at the end of the evolution, we plot in Figure 4 the Wigner function [24] of the projected state into the two eigenstates of the Pauli operator σ_x. The appearance of a single spot with interference patterns indicates that the field is a superposition of two coherent states but with different weights. The explanation of this behavior is as follows. Let us start first by ignoring the term H_{err}. By choosing the initial state (3.5) the state evolves along an adiabatic path in the squeezed-light frame due to the shortcuts to adiabatic method is given by

$$|\psi(t)\rangle = \frac{1}{\sqrt{2}}\left(|+\rangle_x|-\eta(t)\rangle + |-\rangle_x|\eta(t)\rangle\right), \tag{3.6}$$

where the evolution of $\eta(t)$ is obtained from the solution of the following set of differential equations [27]

$$\mathrm{Re}[\dot{\eta}(t)] = \Delta\ \mathrm{Im}[\eta(t)]\,\mathrm{sech}[2r(t)], \tag{3.7a}$$

$$\mathrm{Im}[\dot{\eta}(t)] = \frac{g}{2}\exp[r(t)] - \Delta\mathrm{Re}[\eta(t)]\mathrm{sech}[2r(t)]. \tag{3.7b}$$

Now, if the contribution of term H_{err} is small but not negligible, one can find that the state

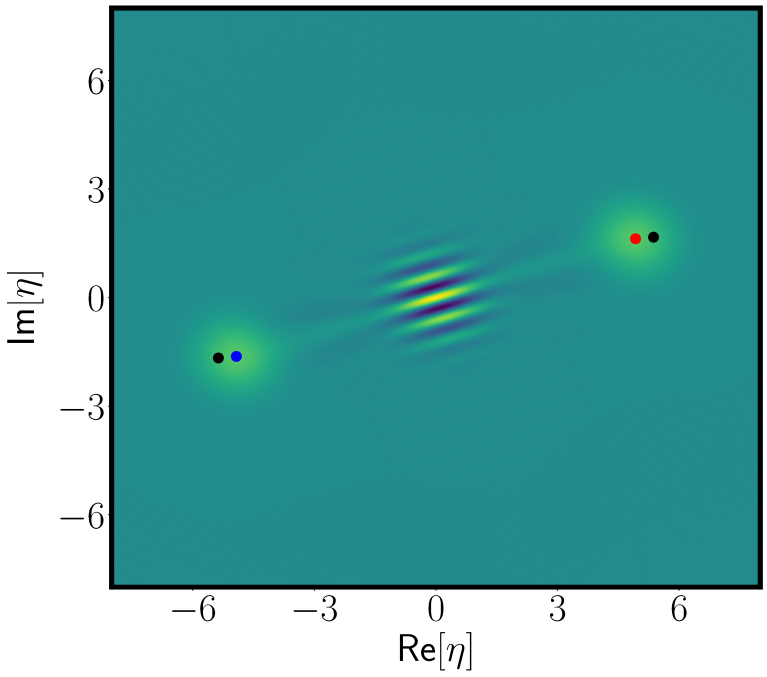

Figure 5. Wigner function of the projection on the state $|g\rangle$ for the coupling strength $g = 0.3$. The red (blue) dot corresponds to actual coherent state $|\eta\rangle$. The two black dots correspond to the solution of the differential equations (3.7). There is a little shift to the solution of the differential equations due to the presence of a non negligible H_{err}.

approximately evolves to

$$\begin{aligned} |\psi(t)\rangle \quad &\approx \quad \frac{1}{\sqrt{\mathcal{N}}}\left(|+\rangle_x\left[|-\eta(t)\rangle - i\epsilon|\eta(t)\rangle\right] + \right. \\ &\left. |-\rangle_x\left[|\eta(t)\rangle - i\epsilon|-\eta(t)\rangle\right]\right), \end{aligned} \tag{3.8}$$

where $\mathcal{N}$ is a real number that normalizes the state (3.8) and $\epsilon \to 0$ for very small value of g/Δ. It is clear from the last equation that the projection on the two eigenstates of the Pauli matrix σ_x involve a superposition of both coherent states $|\pm\eta\rangle$. It is worth mentioning here that at the end of the evolution $t = T$, the final state in the lab frame is very close to the one in the squeezed frame due to the fact that $r(T) \to 0$. Hence, the state given by Equation (3.8) at the end of the evolution can be put in the form

$$\begin{aligned} |\psi\rangle_T \quad &\to \quad (1 - i\epsilon)|g\rangle\left[|-\eta\rangle_T + |\eta\rangle_T\right] + \\ &\quad (1 + i\epsilon)|e\rangle\left[|-\eta\rangle_T - |\eta\rangle_T\right], \end{aligned} \tag{3.9}$$

where $|.\rangle_T$ means the state $|.\rangle$ at $t = T$. The two spots shown in Figure 4 are for $g = 0.1$ and $T = 11.57$ which correspond to the states

$$|-\eta\rangle_T - i\epsilon|\eta\rangle_T \quad \text{and} \quad |\eta\rangle_T - i\epsilon|-\eta\rangle_T, \tag{3.10}$$

where we have found numerically that ϵ is approximately 0.22. We should note here that the small

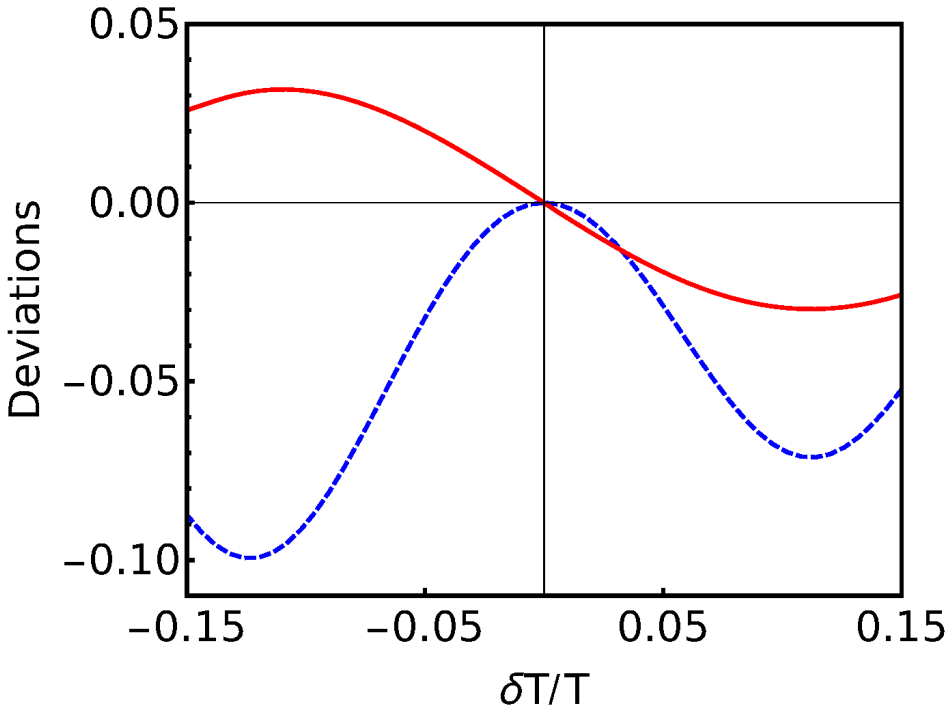

Figure 6. Deviations of the mean photon number $\delta n/n$ (solid line) and logarithmic negativity $\delta E_n/E_n$ (dashed line) as a function of the imperfection in T, taken for the mean photon number $n = 7.23$ at $T = 11.57$.

value of ϵ does not change the cat state size, whether the measurement on the qubit gives the state $|g\rangle$ or $|e\rangle$. However, by increasing the coupling strength g, the contribution of H_{err} increases and leads to the change of the cat state size. This effect is shown in Figure 5 where we plot the Wigner function for the projection of the final state on the qubit state $|g\rangle$ for the coupling strength $g = 0.3$ and $T = 5.25$. It is clear from the figure that the generated entangled cat state is shifted slightly due to the error term H_{err}.

To investigate the robustness against the imperfection of time evolution, we illustrate in Figure 6 the deviations of the mean photon number $\delta n/n$ and the logarithmic negativity $\delta E_n/E_n$ as a function of $\delta T/T$, namely, the imperfection of the time evolution T, using $T = 11.57$ obtained from Figure 3 and assuming that $r(t_f) = 0$ for all $t_f > T$ with the final time $t_f = T\,(1 + \delta T/T)$. It is clear from the figure that the deviation is less than 5% for the mean photon number and that the logarithmic negativity is always decreasing, but not more than approximately 10%. This arises from the fact that the collapse and revival curves in Figure 3b are tangent and close to each other, around T = 11.57. Consequently, we can conclude that our generalized shortcuts to adiabaticity is robust against the imperfection of time evolution.

4. The effect of decoherence

Up to this point, we have assumed an isolated system. However, in reality there will always be interaction with the environment. This interaction can be described by the well known master

equation [27, 40]. In the lab frame it is written as follows:

$$\begin{aligned}\dot{\rho}(t) &= i\left[\rho(t)\,, H_0(t)\,\right] \\ &+\frac{1}{2}\left[2L_\gamma\rho(t)L_\gamma^\dagger - L_\gamma^\dagger L_\gamma\rho(t) - \rho(t)L_\gamma^\dagger L_\gamma\right] \\ &+\frac{1}{2}(N+1)\left[2L_\kappa\rho(t)L_\kappa^\dagger - L_\kappa^\dagger L_\kappa\rho(t) - \rho(t)L_\kappa^\dagger L_\kappa\right] \\ &+\frac{1}{2}N\left[2L_\kappa^\dagger\rho(t)L_\kappa - L_\kappa L_\kappa^\dagger\rho(t) - \rho(t)L_\kappa L_\kappa^\dagger\right] \\ &-\frac{1}{2}M\left[2L_\kappa^\dagger\rho(t)L_\kappa^\dagger - L_\kappa^\dagger L_\kappa^\dagger\rho(t) - \rho(t)L_\kappa^\dagger L_\kappa^\dagger\right] \\ &-\frac{1}{2}M^*\left[2L_\kappa\rho(t)L_\kappa - L_\kappa L_\kappa\rho(t) - \rho(t)L_\kappa L_\kappa\right], \end{aligned} \tag{4.1}$$

where ρ is the density operator, $L_\gamma = \sqrt{\gamma}\sigma_-$ and $L_\kappa = \sqrt{\kappa}a$ are the Lindblad collapse operators for the two-level system and the cavity, respectively. The parameter $\gamma(\kappa)$ is the decay rate of the two-level system (cavity) and the parameters N and M characterize the squeezed vacuum

$$N = \sinh^2(r_2) \quad , \quad M = \cosh(r_e)\sinh(r_e), \tag{4.2}$$

where r_e is the squeezing parameter. It is important to keep in mind that the master equation is based on the Born approximation, which assumes that there is no back reaction and only a weak coupling between the squeezed vacuum and the two-level system/cavity. In the case that there is a strong coupling, the master equation should be replaced by the so called global master equation [41].

It is worth mentioning that the use of the squeezed vacuum is to minimize the influence of thermal noise and two-photon correlation noise in the cavity mode. Transforming the master equation (4.1) into the squeezed-light frame and taking the squeezing parameter $r_e = r_{max}$, the master equation (4.1) can be approximated by

$$\begin{aligned}\dot{\rho}_S(t) &= i\left[\rho_S(t)\,, H_S(t)\,\right] + \\ &+\frac{1}{2}\left[2L_\gamma\rho_S(t)L_\gamma^\dagger - L_\gamma^\dagger L_\gamma\rho_S(t) - \rho_S(t)L_\gamma^\dagger L_\gamma\right] \\ &+\frac{1}{2}\left[2L_\kappa\rho_S(t)L_\kappa^\dagger - L_\kappa^\dagger L_\kappa\rho_S(t) - \rho_S(t)L_\kappa^\dagger L_\kappa\right], \end{aligned} \tag{4.3}$$

where, $\rho_S(t)$ is the density operator in the squeezed frame.

Figure 7 shows the fidelity versus $1/\sqrt{C}$, where $C = g^2/\kappa\gamma$ is the cooperativity parameter. For simplicity we assume that the damping rates κ and γ are equal. It is well known that the damping rates reduce the fidelity but, in our case, it is still always greater than 80%, and it is more than 90% for $\kappa = \gamma \leq 2 \times 10^{-3}$, which shows that our model is robust against dissipation.

For experimental realization, the circuit QED systems are good candidates. To implement frequency modulation of the transmission line resonator, a superconducting quantum interface device boundary is applied to the resonator [20–22]. By changing the flux through the loop of the SQUID one

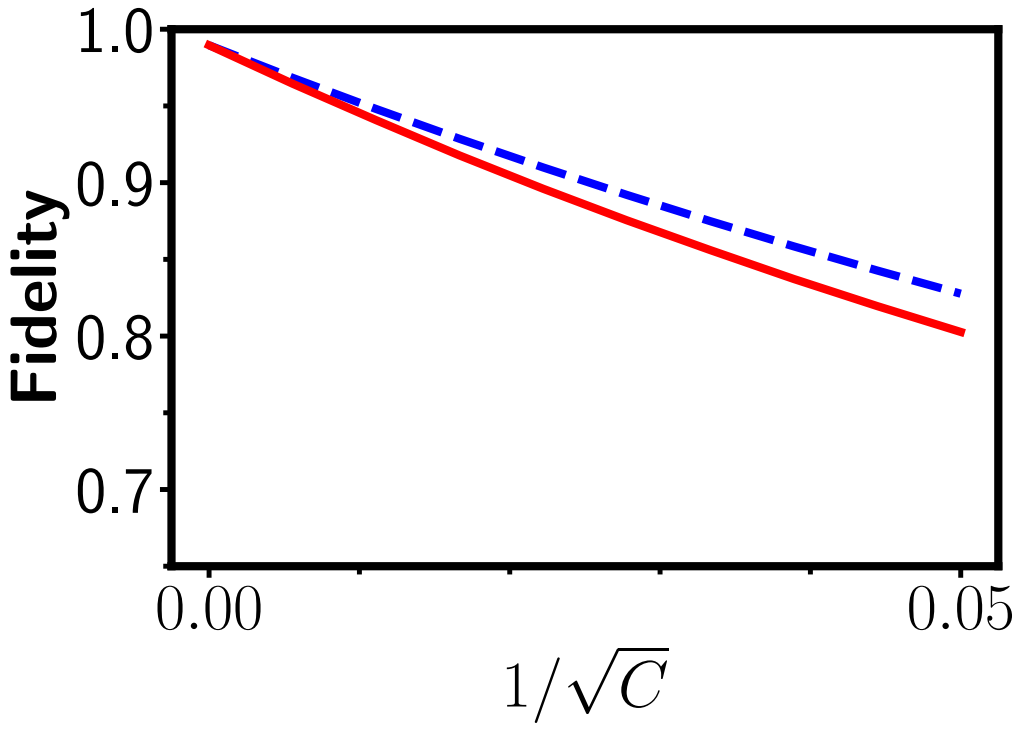

Figure 7. The effect of damping on the fidelity as a function of the $1/\sqrt{C}$, with $C = g^2/\kappa\gamma$ and $\kappa = \gamma$. The values of the parameters are the same as in Figure 6. The solid line corresponds to the master equation (4.1) and the dashed line to Equation (4.3).

can tune the two parameters ξ and ν. The frequency modulation of the two-level system is obtained by adding a σ_z driving with frequency ν, which can be realized experimentally by an external magnetic field that induces a flux driving [17–19]. We choose the low-frequency modulation in order to speed the process. Since the low-frequency modulation is valid for short-time limit, $\nu t \ll 1$ and also because it is more accessible in experiment [16]. A fidelity close to 0.99 can be obtained for smaller values of the driving amplitude $\xi\nu/\omega_a \approx 0.1$.

5. Conclusion

We have investigated how to speed up the generation of entangled states using low-frequency modulations by combining the idea of the ultrastrong JC model [16] with the shortcuts to adiabaticity in Rabi model [27]. This combination, which involves frequency modulations of two-level system and cavity, speeds the generation of giant entangled cat states and increases their size exponentially without losing their robustness against time evolution and dissipation. This approach allows going beyond the conventional ultrastrong coupling regime and simulates the Rabi model using the JC model without the need to have the coupling strength much less than the detuning. We have also studied the effect of the environment and the result shows that our model is robust against dissipation as well as time evolution. In the numerical calculations we concentrate on the value $g = 0.1$, which is the lower limit in the ultrastrong coupling regime; this is because the Hilbert space of the cavity mode grows exponentially as the value of g increases.

Acknowledgments

AM would like to thank Prof. Franco Nori and Dr Ye-Hong Chen for helpful discussions on the shortcuts to adiabaticity used to generate giant entangled cat states. AB would like to thank Prof. Khaled Bouziani for his support and encouragement.

References

[1] I. I. Rabi, "On the Process of Space Quantization," *Physical Review* **49** (1936) 324.

[2] I. I. Rabi, "Space Quantization in a Gyrating Magnetic Field," *Physical Review* **51** (1937) 652.

[3] Z. Ficek, M. R. Wahiddin, "Quantum optics for beginners," Jenny Stanford Publishing, New York (2014).

[4] M. Wagner, "Unitary transformations in solid state physics," North-Holland, Amsterdam (1986).

[5] D. Gerace, S. Portolan, C. Miniatura, L. C. Kwek, A. Auffèves, M. de França Santos, M. Richard, "Strong Light-Matter Coupling: From Atoms To Solid-State Systems," World Scientific, Singapore (2014).

[6] P. Forn-Díaz, L. Lamata, E. Rico, J. Kono J, E. Solano, "Ultrastrong coupling regimes of light-matter interaction," *Reviews of Modern Physics* **91** (2019) 025005.

[7] D. Braak, "Integrability of the Rabi Model," *Physical Review Letters* **107** (2011) 100401.

[8] A. F. Kockum, A. Miranowicz, S. De Liberato, S. Savasta, F. Nori, "Ultrastrong coupling between light and matter," *Nature Reviews Physics* **1** (2019) 19.

[9] A. A. Anappara, S. De Liberato, A. Tredicucci, C. Ciuti, G. Biasiol, L. Sorba, F. Beltram, "Signatures of the ultrastrong light-matter coupling regime," *Physical Review B* **79** (2009) 201303.

[10] T. Schwartz, J. A. Hutchison, C. Genet, T. W. Ebbesen, "Reversible Switching of Ultrastrong Light-Molecule Coupling," *Physical Review Letters* **106** (2011) 196405.

[11] M. Geiser, F. Castellano, G. Scalari, M. Beck, L. Nevou, J. Faist, "Ultrastrong Coupling Regime and Plasmon Polaritons in Parabolic Semiconductor Quantum Wells," *Physical Review Letters* **108** (2012) 106402.

[12] S. J. Bosman, M. F. Gely, V. Singh, A. Bruno, D. Bothner, G. A. Steele, "Multi-mode ultra-strong coupling in circuit quantum electrodynamics," *NPJ Quantum Information* **3** (2017) 46.

[13] A. Bayer, M. Pozimski, S. Schambeck, D. Schuh, R. Huber, D. Bougeard, C. Lange, "Terahertz Light–Matter Interaction beyond Unity Coupling Strength," *Nano letters* **17** (2017) 6340.

[14] F. Yoshihara, T. Fuse, S. Ashhab, K. Kakuyanagi, S. Saito, K. Semba, "Superconducting qubit–oscillator circuit beyond the ultrastrong-coupling regime," *Nature Physics* **13** (2017) 44.

[15] E. T. Jaynes, F. W. Cummings, "Comparison of quantum and semiclassical radiation theories with application to the beam maser," *Proceedings of the IEEE* **51** (1963) 89.

[16] J. F. Huang, J. Q. Liao, L. M. Kuang, "Ultrastrong Jaynes-Cummings model," *Physical Review A* **101** (2020) 043835.

[17] F. G. Paauw, A. Fedorov, C. J. P. M. Harmans, J. E. Mooij, "Tuning the Gap of a Superconducting Flux Qubit," *Physical Review Letters* **102** (2009) 090501.

[18] D. Porras, J. J. García-Ripoll, "Shaping an Itinerant Quantum Field into a Multimode Squeezed Vacuum by Dissipation," *Physical Review Letters* **108** (2012) 043602.

[19] C. Navarrete-Benlloch, J. J. García-Ripoll, D. Porras, "Inducing Nonclassical Lasing via Periodic Drivings in Circuit Quantum Electrodynamics," *Physical Review Letters* **113** (2014) 193601.

[20] J. R. Johansson, G. Johansson, C. Wilson, F. Nori, "Dynamical Casimir Effect in a Superconducting Coplanar Waveguide," *Physical Review Letters* **103** (2009) 147003.

[21] C. M. Wilson, T. Duty, M. Sandberg, F. Persson, V. Shumeiko, P. Delsing, "Photon Generation in an Electromagnetic Cavity with a Time-Dependent Boundary," *Physical Review Letters* **105** (2010) 233907.

[22] C. M. Wilson, G. Johansson, A. Pourkabirian, M. Simoen, J. R. Johansson et al., "Observation of the dynamical Casimir effect in a superconducting circuit," *Nature* **479** (2011) 376.

[23] G. Romero, D. Ballester, Y. M. Wang, V. Scarani, E. Solano, "Ultrafast Quantum Gates in Circuit QED," *Physical Review Letters* **108** (2012) 120501.

[24] H. R. Lewis Jr, W. Riesenfeld, "An Exact Quantum Theory of the Time-Dependent Harmonic Oscillator and of a Charged Particle in a Time-Dependent Electromagnetic Field," *Journal of Mathematical Physics* **10** (1969) 1458.

[25] M. Demirplak, S. A. Rice, "Adiabatic Population Transfer with Control Fields," *The Journal of Physical Chemistry A* **107** (2003) 9937.

[26] E. Torrontegui, S. Ibánez, S. Martínez-Garaot, M. Modugno, A. del Campo et al., "Chapter 2 - Shortcuts to Adiabaticity," *Advances in Atomic, Molecular, and Optical Physics* **62** (2013) 117.

[27] Y. H. Chen, W. Qin, X. Wang, A. Miranowicz, F. Nori, "Shortcuts to Adiabaticity for the Quantum Rabi Model: Efficient Generation of Giant Entangled Cat States via Parametric Amplification," *Physical Review Letters* **126** (2021) 023602.

[28] J. Joo, W. J. Munro, T. P. Spiller, "Quantum Metrology with Entangled Coherent States," *Physical Review Letters* **107** (2011) 083601.

[29] B. Hacker, S. Welte, S. Daiss, A. Shaukat, S. Ritter, L. Li, G. Rempe, "Deterministic creation of entangled atom–light Schrödinger-cat states," *Nature Photonics* **13** (2019) 110.

[30] V. V. Albert, C. Shu, S. Krastanov, C. Shen, R. B. Liu et al., "Holonomic Quantum Control with Continuous Variable Systems," *Physical Review Letters* **116** (2016) 140502.

[31] L. Li, C. L. Zou, V. V. Albert, S. Muralidharan, S. M. Girvin, L. Jiang, "Cat Codes with Optimal Decoherence Suppression for a Lossy Bosonic Channel," *Physical Review Letters* **119** (2017) 030502.

[32] D. Guéry-Odelin, A. Ruschhaupt, A. Kiely, E. Torrontegui, S. Martinez-Garaot, J. G. Muga, "Shortcuts to adiabaticity: Concepts, methods, and applications," *Reviews of Modern Physics* **91** (2019) 045001.

[33] M. V. Berry, "Transitionless quantum driving," *Journal of Physics A: Mathematical and Theoretical* **42** (2009) 365303.

[34] A. del Campo, "Shortcuts to Adiabaticity by Counterdiabatic Driving," *Physical Review Letters* **111** (2013) 100502.

[35] R. Y. Yan, Z. B. Feng, M. Li, C. L. Zhang, Z. Y. Zhao, "Speeding up the Generation of Entangled State between a Superconducting Qubit and Cavity Photons via Counterdiabatic Driving," *Annalen der Physik* **532** (2020) 1900613.

[36] L. H. Du, X. F. Zhou, Z. W. Zhou, X. Zhou, G. C. Guo, "Generalized Rabi model in quantum-information processing including the $\vec{A}^2$ term," *Physical Review A* **86** (2012) 014303.

[37] A. Blais, R. S. Huang, A. Wallraff, S. M. Girvin, R. J. Schoelkopf, "Cavity quantum electrodynamics for superconducting electrical circuits: An architecture for quantum computation," *Physical Review A* **69** (2004) 062320.

[38] J. B. Clark, F. Lecocq, R. W. Simmonds, J. Aumentado, J. D. Teufel, "Sideband cooling beyond the quantum backaction limit with squeezed light," *Nature* **541** (2017) 191.

[39] H. Vahlbruch, D. Wilken, M. Mehmet, B. Willke, "Laser Power Stabilization beyond the Shot Noise Limit Using Squeezed Light," *Physical Review Letters* **121** (2018) 173601.

[40] M. O. Scully, M. S. Zubairy, "Quantum Optics," Cambridge University Press, Cambridge (1997).

[41] A. Levy A, R. Kosloff, "The local approach to quantum transport may violate the second law of thermodynamics," *Europhysics Letters* **107** (2014) 20004